water

MDPI

Article

Analyzing the Effect of Ocean Internal Variability on Depth-Integrated Steric Sea-Level Rise Trends Using a Low-Resolution CESM Ensemble

Emily Hogan * and Ryan Sriver

Department of Atmospheric Sciences, University of Illinois at Urbana-Champaign, Champaign-Urbana, IL 61801, USA; rsriver@illinois.edu

* Correspondence: eehogan2@illinois.edu; Tel.: +1-217-333-2046

Received: 14 March 2017; Accepted: 27 June 2017; Published: 1 July 2017

Abstract: Ocean heat uptake is a key indicator of climate change, in part because it contributes to sea-level rise. Quantifying the uncertainties surrounding ocean heat uptake and sea-level rise are important in assessing climate-related risks. Here, comprehensive global climate model ensembles are used to evaluate uncertainties surrounding decadal trends in depth-integrated global steric sea-level rise due to thermal expansion of the ocean. Results are presented against observational estimates, which are used as a guide to the state of recent literature. The first ensemble uses the Community Earth System Model (CESM), which samples the effects of internal variability within the coupled Earth system including contributions from the sub-surface ocean. We compare and contrast these results with an ensemble based on the Coupled Model Intercomparison Project Phase 5 (CMIP5), which samples the combined effects of structural model differences and internal variability. The effects of both internal variability and structural model differences contribute substantially to uncertainties in modeled steric sea-level trends for recent decades, and the magnitude of these effects varies with depth. The 95% range in total sea-level rise trends across the CESM ensemble is 0.151 mm·year^{-1} for 1957–2013, while this range is 0.895 mm·year^{-1} for CMIP5. These ranges increase during the more recent decade of 2005–2015 to 0.509 mm·year^{-1} and 1.096 mm·year^{-1} for CESM and CMIP5, respectively. The uncertainties are amplified for regional assessments, highlighting the importance of both internal variability and structural model differences when considering uncertainties surrounding modeled sea-level trends. Results can potentially provide useful constraints on estimations of global and regional sea-level variability, in particular for areas with few observations such as the deep ocean and Southern Hemisphere.

Keywords: climate variability; Earth System Modeling; sea-level rise

1. Introduction

Steric sea-level change, due primarily to thermal expansion of seawater, is a major contributor to global sea-level rise estimates. Recent observational analyses indicate that thermosteric contributions account for nearly 40% of total global sea-level rise since ~1970 [1] as approximately 93% of the 1970–2010 additional heat added to the climate system has been stored in the ocean [2]. However, there are potentially large uncertainties due to lack of ocean temperature observations, particularly for the deep ocean (below 2000 m) [1,3–5], and in the Southern Hemisphere, where observational coverage is sparse [6–13]. Uncertainties in both observed and modeled sea-level change can influence interpretations about sea-level rise risks [14–16], such as flooding, increased storm surge and coastal erosion [1,16,17]. In addition, characterising the relative contributions of different integrated ocean depths to steric sea-level rise can provide important insights about the vertical structure of ocean

heat uptake and storage [18,19] and how these are influenced when considering the effects of both anthropogenic climate change and natural variability within the coupled system [20].

Coupled climate models are useful tools to assess and aid understanding about anthropogenic and natural climate variability [21–23]. Different types of model ensembles can capture different types of uncertainties. For example, the Coupled Model Intercomparison Project Phase 5 (CMIP5) is comprised of multiple different global climate models (GCMs), which follow identical forcing pathways for historical and future projections. Thus, differences in results between models for the same time-varying forcing arise due to variations in model structure, complexity, spatial resolution and initial conditions [24]. We can also use single-model ensembles to isolate the effect of initial conditions uncertainty and unforced internal variability. Examples of these include the Community Climate System Model Version 3 (CCSM3) ensemble [25], the Community Earth System Model Large Ensemble (CESM LENS) [26] and a recent low resolution coupled CESM-Initial Conditions Ensemble [27]. These types of ensembles are useful for analysing the effects of internal variability on past/future climate trends [28].

Internal variability is due to innate non-linear dynamical processes within the climate system that occur in the absence of external forcing [25]. Contributing factors to internal variability include several different types of climate oscillations, such as the El Nino Southern Oscillation (ENSO) [29], the Pacific Decadal Oscillation and Atlantic Multidecadal Oscillation [30]. Internal variability can influence interpretations about anthropogenic climate change and has been put forward as a cause of the recent global warming hiatus [31–35]. Interestingly, during this recent period of decreased warming, the deep-ocean is thought to have taken up significantly more heat [32] and timeseries of global ocean heat content suggest persistent ocean warming during recent decades [36].

We can simulate the effect of internal variability in single-model climate change ensembles by initializing each ensemble member using different initial conditions [22], either in the atmosphere [26] or the coupled ocean–sea–ice–land–atmosphere system [23]. This unforced variability can affect climate patterns on interannual-to-decadal timescales, and determine ensemble spread of key climate properties in historical and future simulations. The effect of internal variability is often amplified with decreasing spatial and temporal scales [23,37–39] and can contribute significantly to variations in regional climate on inter-seasonal to inter-decadal timescales.

In this study, two comprehensive global climate model ensembles are used to diagnose and report the vertical structure of global steric sea-level trends for recent decades. We highlight results from a new 50-member CESM ensemble that varies initial conditions to internal variability within the coupled ocean–atmosphere system [23]. In addition, we analyze results from 32 different CMIP5 models (1 simulation from each model). This ensemble highlights uncertainties due to both different model structures and internal variability.

The main focus of this paper is to quantify the effect of oceanic internal variability on sea-level trend estimates using a self-consistent and fully-coupled modeling framework, and we compare and contrast results with CMIP5 models sampling primarily structural model differences as a guide for comparing relative importance of internal variability for a single-model ensemble versus multi-model ensemble analysis. Results are framed within the broader context of observational estimates and uncertainties of steric sea-level rise from the National Center for Environmental Information (NCEI) [40,41]. The paper is organized as follows. Section 2 presents and describes in detail the materials and methods including the ensemble analysis. In Section 3 we outline the main results and discussion, and Section 4 presents some conclusions and implications.

2. Materials and Methods

We present results from a new 50-member climate change ensemble experiment using the low-resolution version of CESM, a fully-coupled, global climate model [42,43]. The model configuration is based on version CESM1.03, and features an atmospheric component (CCSM4) with T31 spectral resolution (~3.75° × 3.75°) and 26 vertical levels. The model ocean component is the Parallel Ocean

Program version 2 [44] with a nominal horizontal grid resolution of 3°, which decreases to less than 1° at the equator. The ocean model contains 60 vertical levels, down to a maximum depth of 5500 m.

The experiment used in this study was designed to sample internal variability in the model-coupled Earth system, including the deep ocean [23]. First, we spun up a fully coupled control simulation with constant pre-industrial radiative forcing. Beginning at the year 4200, after the deep ocean had reached approximate dynamic equilibrium, historical simulations with transient natural and anthropogenic forcings were initialized from unique snapshots of the fully coupled model state sampled every 100 years from the control simulation, ending with 50 ensemble members. The transient simulations are extended to 2100 using the representative concentration pathway (RCP) 8.5, an idealized future scenario in which anthropogenic radiative forcing increases to roughly 8.5 W m^{-2} by 2100 [45]. Allowing the ocean to reach approximate dynamic equilibrium prior to initializing the climate change ensemble prevents any model ocean drift from affecting our estimates of sea-level variability. Even after ~4000 years of equilibration, the model exhibits small drift in the deep ocean and internal variability across a variety of timescales (interannual to centennial). As a simple illustration, Figure 1 displays the timeseries of ocean temperature in the pre-industrial control simulation at a depth of 2000 m in the North Pacific (Latitude: 57° N, Longitude: 180° W) over the period which our 50-member ensemble runs are initialized (equilibration year 4200–9100). The North Pacific deep ocean contains some of the oldest waters on the planet, as this area has little deep-water formation or upwelling. Even after the ~4000-year spin up, we still see a small trend in ocean temperature in the presence of relatively large internal variability, during the next 5000 years (model year 4000–9000).

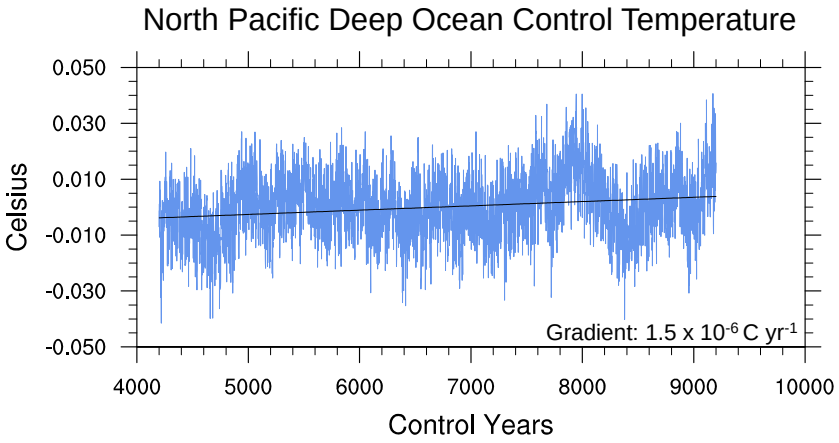

Figure 1. Ocean temperature at 57° N, 180° W, 2000 m depth in the Community Earth System Model (CESM) pre-industrial control simulation, from model year 4000 to 9200, the time period over which transient historical and representative concentration pathway (RCP) simulations are initialized. The timeseries is offset by the average over the control period. The black line shows the linear trend over the 5200 years, and its gradient is inset in the bottom right corner.

The low-resolution version of CESM was chosen for this ensemble due to its computational tractability. The deep ocean requires several thousand years to reach approximate equilibrium, which is difficult to achieve using higher resolution and more computationally expensive models. The low resolution CESM helps mitigate this computational tradeoff, given that it has been shown to capture key aspects of the climate variability [23,42,46], though the model also exhibits significant biases. This version of the model has low heat transport leading to a cool sea surface temperature bias and problems with excessive sea ice extent and thickness in the North [42]. In addition, CESM has no interactive aerosols in the atmospheric component of the model, which may lead to warm biases in different model variables [21,47]. These issues should be taken into account when looking at sea-level rise trends in the low-resolution version of the model, though in the case of this study, where we focus on characterizing the effect of internal variability on sea-level rise trends, model skill is of less significance.

Large ensemble experiments have been performed using higher resolution versions of CESM, for example the LENS ensemble, that has approximately 1° horizontal resolution in all model components [26]. However, the recent LENS ensemble initializes its transient runs differently from our ensemble. Differences in initial conditions in the LENS ensemble are created by perturbing atmospheric temperature at each grid point at the 12th decimal place. The initial conditions for the other model components (e.g., the ocean) are identical for all ensemble members. With an identical ocean for the initialization of each simulation, LENS does not sample ocean internal variability.

The effect of these different initialization strategies on surface atmosphere temperature and volume-weighted ocean temperature are shown in Figures 2 and 3. In these figures, we show our fully equilibrated CESM ensemble (CESM-AO, where AO points to the sampling of both atmosphere and ocean) in which we initialize each historical hindcast ensemble member by sampling the joint internal variability of the atmosphere and ocean. We also performed a "LENS equivalent" experiment with the low-resolution version of CESM (CESM-A, where the A points to the sampling of the atmosphere only), where we initialized 40 hindcast simulations from a constant ocean state, and we perturb atmospheric temperature consistent with the LENS method to create small differences in the initial conditions reflecting internal variability of the atmosphere.

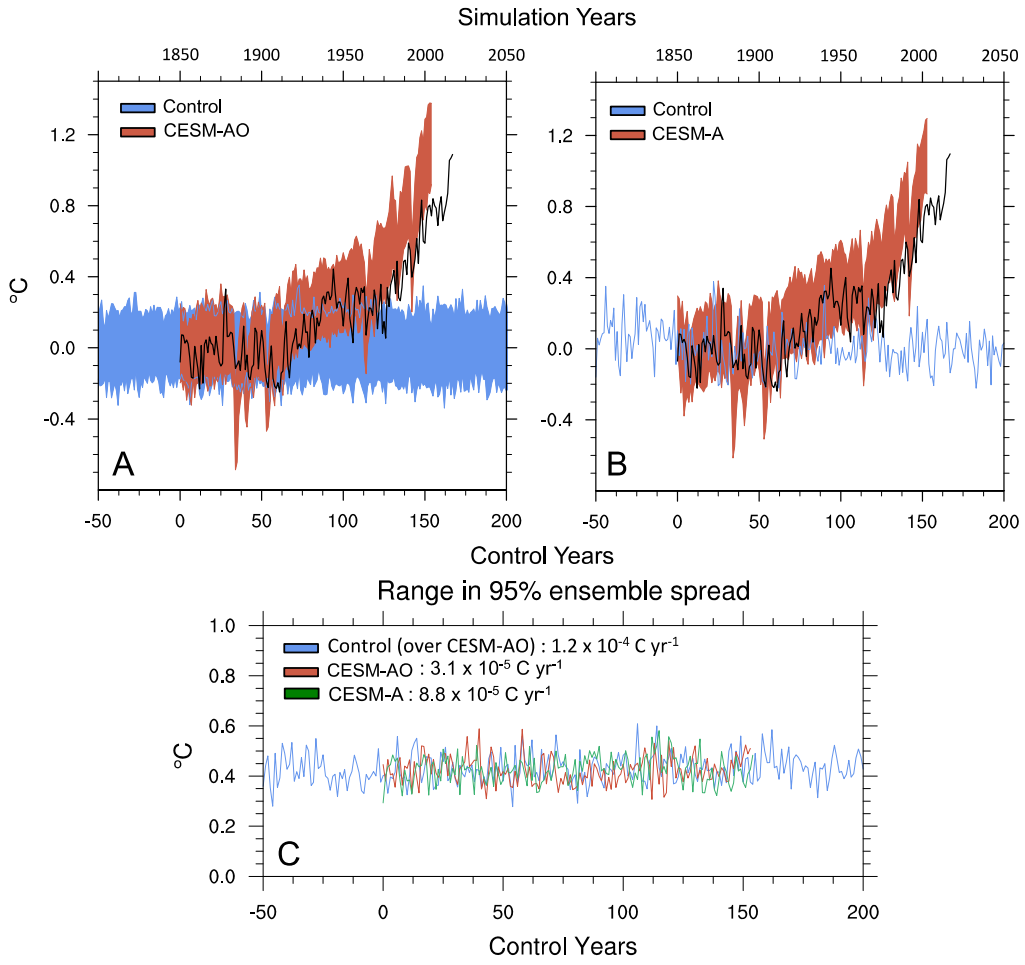

Figure 2. Globally averaged atmospheric surface temperature for CESM-AO (**A**) and CESM-A (**B**). See text for description of differences between ensembles. Blue lines (**A**,**B**) display timeseries of atmospheric temperature pre-industrial control simulation. Red lines display historically forced simulations. The 95% range in ensemble spread is shown in (**A**) and (**B**). Black lines are observed globally average temperature from the HadCRUT4 dataset [48]. Timeseries of the 95% range are shown in (**C**). Values are the linear trend in ensemble spread over the period shown from 0–150 years.

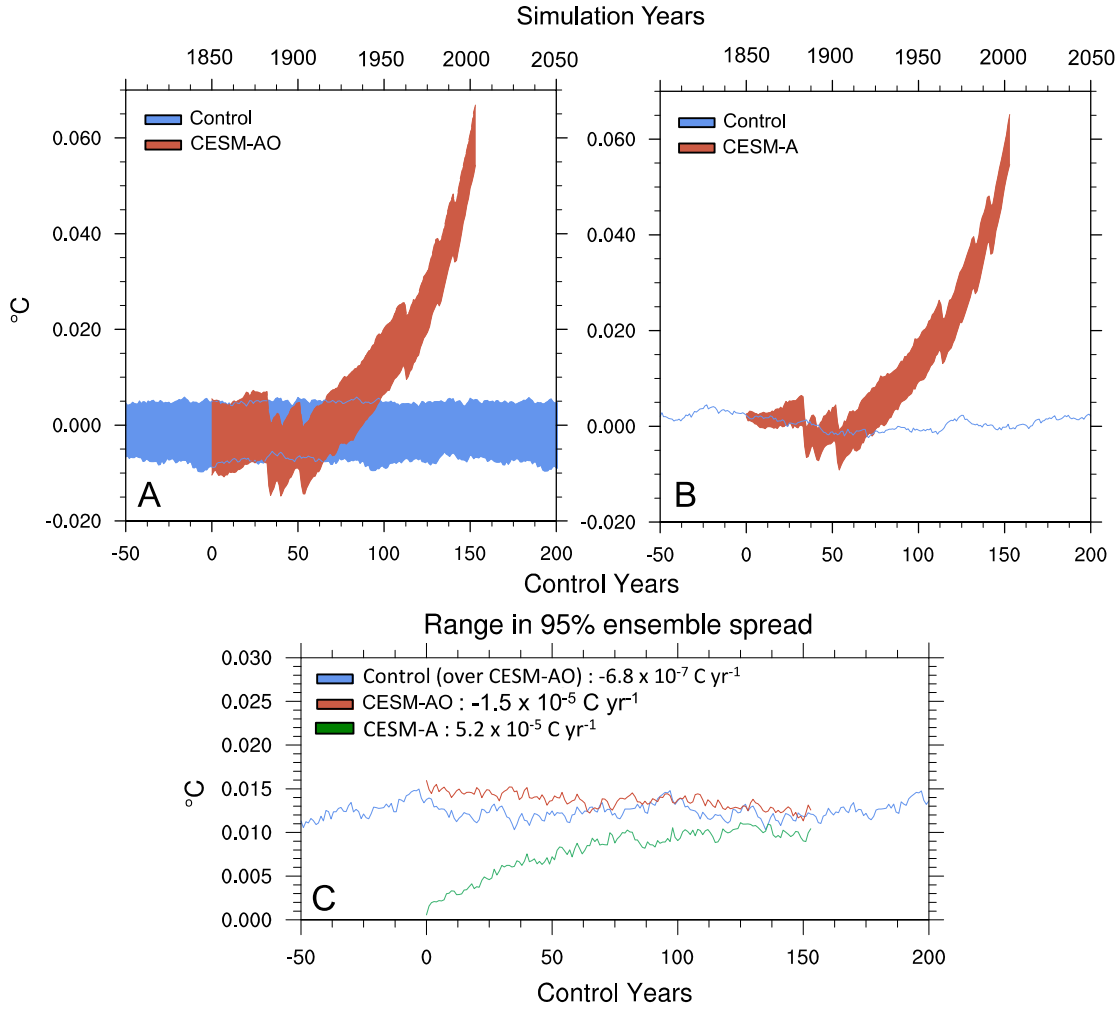

Figure 3. Globally averaged ocean temperature for CESM-AO (**A**) and CESM-A (**B**). See text for description of differences between ensembles. Blue lines (**A**,**B**) display timeseries of the oceanic temperature pre-industrial control simulation. Red lines (**A**,**B**) display historically forced simulations. The 95% range in ensemble spread is shown in (**A**) and (**B**). Timeseries of the 95% range are shown in (**C**). Values are the linear trend in ensemble spread over the period shown from 0–150 years.

Figure 2 shows globally averaged atmospheric surface temperature from 1850–2005 for both CESM-AO (Figure 2A) and CESM-A (Figure 2B). As each run from CESM-AO is initialized from its own point in the control run, we have 50 segments of control plotted against each of the 50 historical simulations. Each run from CESM-A was initialized from the same point in the control (year 7000). As the atmosphere equilibrates on relatively short timescales (e.g., months), the historical simulations in each panel show very similar ranges of variability over the whole historical period (Figure 2C). In order to sample atmospheric variability, an ensemble experiment such as CESM-A, or LENS, would therefore be appropriate.

Globally averaged oceanic temperature is shown in Figure 3, for CESM-AO (Figure 3A) and CESM-A (Figure 3B). The difference between the two ensembles is obvious in the first 25 years of the historical simulations, where variability in ocean temperature in CESM-A is a fraction of the total variability in CESM-AO. By the end of the simulations in 2005, variability in CESM-A has not reached the range of that seen by CESM-AO. This effect is magnified when focusing specifically on the deep ocean (not shown). The relatively longer adjustment timescale of the ocean reflects its long memory and thermal inertia compared to the atmosphere. In the CESM-A ensemble, the low frequency variability of all ensemble members tends to follow the control simulation for the first several decades,

and the range of internal variability increases with time (Figure 3C). Thus, in order to achieve a robust characterization of the full internal variability of the ocean, we use an equilibration and ensemble initialization strategy using the fully-coupled model (CESM-AO). Ensembles such as CESM-A or LENS are perhaps not appropriate for inferring sub-surface ocean variability given the limitations in sampling the internal variability of the ocean. In addition, Figure 3C shows that the internal ocean temperature variability for CESM-AO also decreases with time in response to increasing anthropogenic forcing. Thus, sampling internal variability from a long pre-industrial control simulation (and super-imposing it on the estimated trends) would also not be appropriate, since that implicitly assumes the variability is a stationary process.

The second ensemble consists of 32 different models used in the Coupled Model Intercomparison Project phase 5 (CMIP5) [24]. See Appendix A for the list of CMIP5 models used in this study. One simulation (r1i1p1) was used from each model corresponding to a historical hindcast that runs through to the end of 2004 (1850–2005) and projections (2005–2100) using the RCP 8.5 forcing scenario [46]. Using one simulation from each model creates an ensemble that samples primarily the effect of different model structures and minimizes the effect of internal variability (though the two effects cannot be completely separated since each model uses unique initial conditions for the historical hindcasts). The CMIP5 database is used widely by the scientific community to analyse climate change and variability. We use it here as a guide to compare and contrast the effect of different sources of variability (internal versus structural + internal) for the sub-surface ocean.

Steric sea-level change in the CMIP5 is estimated from the inverse of the ocean density field [14,49]. Ocean density in each model is calculated using the equation of state of seawater based on potential temperature and salinity [50]. During post-processing of the temperature and salinity fields, we found significant ocean drift at all depths in many of the CMIP5 models [51–53]. This drift is not present in the CESM ensemble, which is based on a ~10,000 year fully coupled pre-industrial equilibrium simulation (Figure 1). We corrected for the sub-surface ocean drift in each of the CMIP5 models by first calculating the linear trend in density at every model grid point in the pre-industrial control simulations. Each CMIP5 model had a different length of control available, so we used all that were available to calculate the trends in order to correct for drift as accurately as possible. We then subtracted these trends at each grid point from the historical hindcasts and projections. Models with non-linear or oscillatory sea-level drift in the pre-industrial control runs were not used in the analysis. This method of subtracting relative drift at each grid point allows the analysis of both regional and depth-dependent steric sea-level changes, which enables us to assess contributions from the deep ocean.

Observed steric sea-level change down to a depth of 2000 m was downloaded from the National Center for Environmental Information (NCEI) [40,41]. Pentadal anomalies were used for the period 1957–2013, and yearly anomalies used for the full period of their availability: 2005–2015. Other studies have examined the uncertainty in observed sea-level change due to different biases and a lack of global coverage by documenting several sources of observations [11,12]. In this study, we choose to use only NCEI as a reference for assessing ensemble variability and differences. We have previously noted that both the models and observations exhibit biases and uncertainties, and it is important to keep these biases in mind when comparing with model results. We use two different time periods for analysing sea-level trends in order to compare the effects of internal variability and structural model differences over both decadal and multi-decadal timescales, and over different ocean depths.

3. Results and Discussion

We analyse global steric sea-level trends and variability for decadal and multi-decadal time periods (Figure 4) to diagnose the effects of internal variability and different model structures from various ocean depths.

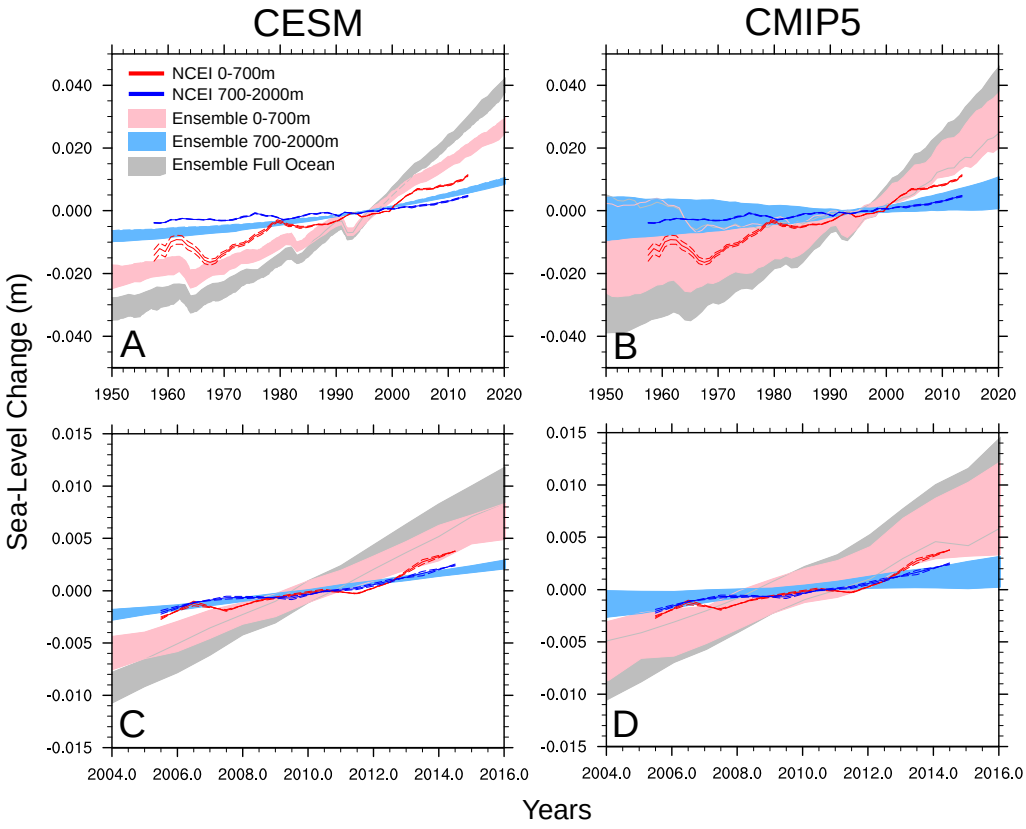

Figure 4. Timeseries of 95% model ensemble range of steric sea-level change over different ocean depths. Observations from National Center for Environmental Information (NCEI) are overlaid, with dashed lines displaying uncertainty provided by the dataset. (**A**) and (**B**) display all available pentadal observations (1957–2013). (**C**) and (**D**) zoom in on yearly observations (2005–2015). Data is offset by the 1986–2005 average in (**A**) and (**B**). Data is offset by the 2005–2015 average in (**C**) and (**D**). Full ocean is defined as the entire available depth of each model ocean.

We show observational estimates as a reference for ensemble comparisons [40,41], keeping in mind the inherent uncertainties and limitations in both the model and observations. Pentadal observations are used from 1957–2013, and yearly observations are used from 2005–2015 from NCEI. All panels display the 95% range of each ensemble. Both the CESM and CMIP5 ensembles exhibit larger mean sea-level rise in the upper ocean compared to NCEI, which may be an artefact of several different types of biases in both models and observations. Model biases in CESM are discussed in the previous section with issues relating to the low-resolution version used. Discrepancies in the higher-resolution models that make up the CMIP5 ensemble may be due to multiple reasons, but the warm biases seen here in the ensemble may be due to a lack of interactive aerosols in some of the models included in the ensemble [21,47]. As a simple test to characterize the effect of aerosols on steric sea-level rise, we calculated trends in the CMIP5 models included in this study with and without interactive aerosols (those with interactive aerosols are highlighted in bold in Appendix A) and compared these to the trends of those that did not. Table 1 shows how the mean ensemble sea-level trends decrease when considering only models with interactive aerosols, but that this effect is only pronounced on multi-decadal timescales. Additionally, the observations themselves may not represent true sea-level change, as ocean coverage is poor throughout the subsurface ocean and observations are biased towards the Northern Hemisphere, as coverage in the South is far less extensive [6–13].

Table 1. Mean steric sea-level rise in Coupled Model Intercomparison Project Phase 5 (CMIP5) models, split into those models that have interactive aerosol chemistry (Interactive), and those that do not (non-interactive).

Mean (mm·year^{-1})	1975–2013		2005–2015	
	Interactive	Non-Interactive	Interactive	Non-Interactive
0–700 m	0.454	0.655	1.153	1.053
700–2000 m	0.057	0.152	0.270	0.275
Full Ocean	0.579	0.871	1.546	1.419

The comparison of steric sea-level trends in CESM over the different depths show that the majority of thermal expansion and total spread due to internal variability in the model ocean occurs closest to the surface, between 0–700 m depth. The uncertainties vary over different timescales: Figure 5 displays histograms of trends over the longer period, while Figure 6 shows trends over the most recent available decade, 2005–2015. The ensemble means are presented in Table 2, and we quantify uncertainty due to internal variability in CESM over different depths in Table 3. Internal variability contributes significantly to uncertainty in CESM trends, particularly in the upper ocean where we see a range of 0.117 mm·year^{-1} in the upper ocean, out of the total of 0.151 mm·year^{-1} range throughout the full ocean for the multi-decadal period. As expected, the range in trends is larger for CMIP5 than for the CESM ensembles over all depths and time periods, indicating that the effect of structural model differences + internal variability over multiple models is larger than that for internal variability in CESM for these timescales. Over the full ocean during the multi-decadal time period, we estimate a range of 0.151 mm·year^{-1} in CESM to a range of 0.895 mm·year^{-1} in CMIP5. From 2005–2015, we see a range of 0.509 mm·year^{-1} for CESM, to a range of 1.470 mm·year^{-1} in CMIP5. Table 3 also shows that variability in sea-level rise trends is larger during the more recent period (also seen in Figure 6) for both ensembles and for all integrated depths. The contribution from internal variability (CESM) in the full ocean over the longer period is approximately 17% of the variability seen in CMIP5, but this value increases to 46% over the shorter period. This increase in variability in CESM to a greater magnitude than in CMIP5 is consistent with previous studies showing that the effect of internal variability can be amplified on shorter timescales of ~10 years [37–39]. As a separate simple experiment, we have examined the vertical structure of steric sea-level rise (a proxy for ocean heat uptake) in the model ensembles using identical time periods to recently published observational estimates that include contributions from the deep ocean (2005–2013, hereafter the "Llovel period") [3]. The referenced study calculates and provides estimates of steric ocean rise over the Llovel period for similar ocean depths (0–700 m and 700–2000 m), and also for the deep ocean (below 2000 m). This was done using a sea-level budget approach. Trends found via Argo [54], and the Gravity Recovery and Climate Experiment (GRACE) [55], are subtracted from trends obtained by satellite altimetry [56]. We use these data to examine whether our ensemble sampling internal variability fit within the range of observational uncertainty calculated using this sea-level budget method. Over the Llovel period for the depths of 0–700 m, both CESM and CMIP5 show mean trends of 1.05 mm·year^{-1}, which are considerably larger than the observational estimate (0.53 mm·year^{-1}). At mid-levels (700–2000 m), modeled values of 0.4 mm·year^{-1} for CESM, and 0.27 mm·year^{-1} for CMIP5 are more consistent with the observational estimate (0.38 mm·year^{-1}). The relatively low values in CMIP5 models at these mid-levels are consistent with previous results [52]. Using the sea-level budget approach, the calculated global observed trend below 2000 m is found to be −0.13 mm·year^{-1}. This negative sea-level trend implies deep ocean cooling, with large uncertainty. In contrast, we calculated 0.12 mm·year^{-1} for CESM, and 0.1 mm·year^{-1} for CMIP5 during this time period. The ensembles show a lower range in spread over these depths than in the upper ocean (not shown). Considering the model/data discrepancies, the spread in both model ensembles are within the range of uncertainty based on this calculated observational estimate [3]. Some CMIP5 models also exhibit negative sea-level change (e.g., cooling) in

the deep ocean. The observed ranges were considered conservative due to observational limitations, prompting recent discussion on whether this negative trend is the result of deep ocean cooling, or perhaps due to the uncertainties in the sea-level budget [3,57,58]. Differences in deep ocean values between observed and modeled steric sea-level may also be due to a lack of observed data below 2000 m [54], and due to discrepancies in modeled temperature diffusion.

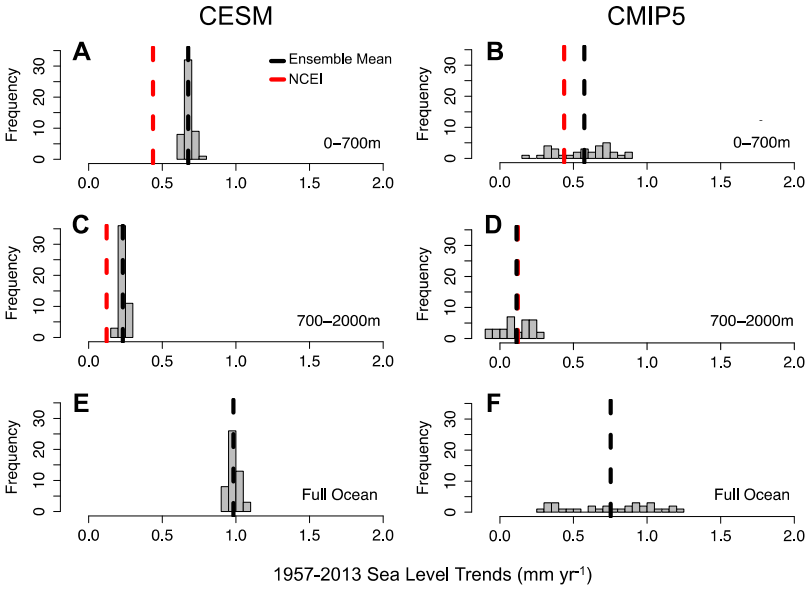

Figure 5. Histograms of model ensemble steric trends over different depth for the multi-decadal period (1957–2013). Full ocean is defined as the entire available depth of each model ocean. Red dashed lines are observations from the National Center for Environmental Information (NCEI), and black dashed lines are the model ensemble means. (**A**): CESM, 0–700 m; (**B**): CMIP5, 0–700 m; (**C**): CESM, 700–2000 m; (**D**): CMIP5, 700–2000 m; (**E**): CESM, Full ocean; (**F**): CMIP5, Full ocean.

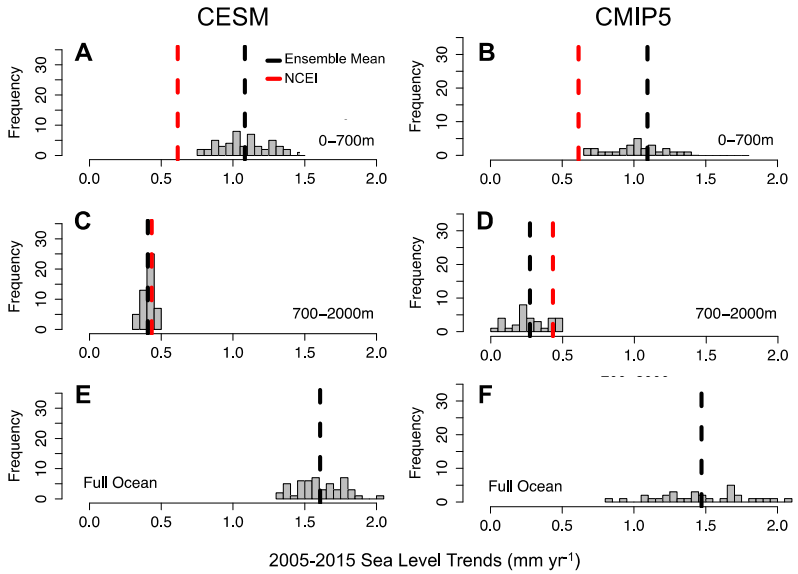

Figure 6. Histograms of model ensemble steric trends over different depths for the decadal period (2005–2015). Full ocean is defined as the entire available depth of each model ocean. Red dashed lines are observations from NCEI, and black dashed lines are the model ensemble means. (**A**): CESM, 0–700 m; (**B**): CMIP5, 0–700 m; (**C**): CESM, 700–2000 m; (**D**): CMIP5, 700–2000 m; (**E**): CESM, Full ocean; (**F**): CMIP5, Full ocean.

Table 2. Ensemble mean trends in steric sea-level rise for both periods and ensembles over all evaluated depths.

Mean ($mm \cdot year^{-1}$)	1975–2013		2005–2015	
	CESM	CMIP5	CESM	CMIP5
0–700 m	0.676	0.573	1.083	1.094
700–2000 m	0.232	0.113	0.407	0.273
Full Ocean	0.983	0.753	1.607	1.470

Table 3. 95% range in ensemble steric sea-level rise trends for both periods and ensembles over all evaluated depths.

Mean ($mm \cdot year^{-1}$)	1975–2013		2005–2015	
	CESM	CMIP5	CESM	CMIP5
0–700 m	0.117	0.597	0.573	0.993
700–2000 m	0.081	0.342	0.126	0.436
Full Ocean	0.151	0.895	0.509	1.096

As expected, the difference in the range of uncertainty for global trends in steric sea-level change between CESM and CMIP5 is substantial (Figures 4–6, Tables 2 and 3). Analysis of steric sea-level rise (SLR) trends in climate models can provide useful diagnostic model information as well as guide assessments, but diagnosing regional trends and variability is perhaps more important to decision makers, since major damages (e.g., floods) tend to occur over relatively small scales [59]. We highlight variability in both model ensembles for different locations in Figure 7, calculating and displaying steric change for the ocean grid cells closest to these locations over the decadal time period of 2005–2015. Note that the CMIP5 models are drift-corrected at every point, minimizing potential regional biases (see Methods section). Figure 7 illustrates the importance of internal variability as it shows that on regional scales, the combination of structural model differences and internal variability in CMIP5 is of a comparable magnitude as internal variability in CESM. This demonstrates that the effect of coupled internal variability (CESM) increases with smaller spatial scales in sea-level rise, consistent with other examined atmospheric variables [23,37–39]. This illustrates the challenge in distinguishing forced responses to internal unforced variability within the sub-surface ocean using multi-model and initial condition climate model ensembles.

Figure 8 demonstrates how the effect of internal variability may impact the projections of sea-level rise estimates, using the northeastern coast of the United States as a reference. The plot shows different estimates of regional steric plus dynamic sea-level rise in the year 2100 from the CESM ensemble using the ensemble mean global average sea-level change (dashed green line), the ensemble mean sea-level change for the northeastern US (dashed black line), and the upper limit of the ensemble taking into account the model's internal variability (red line). As seen in Figure 8, accounting for internal variability on a regional scale could increase the projection of the upper bound of sea level rise by an extra 10% for this region. Characterizing uncertainties surrounding internal variability can provide useful information to diagnose potential upper bounds of sea-level rise, taking into account vertical structure of ocean heat uptake and horizontal structure of ocean heat transport. In turn, this information can assist coastal planning and investment decisions [59].

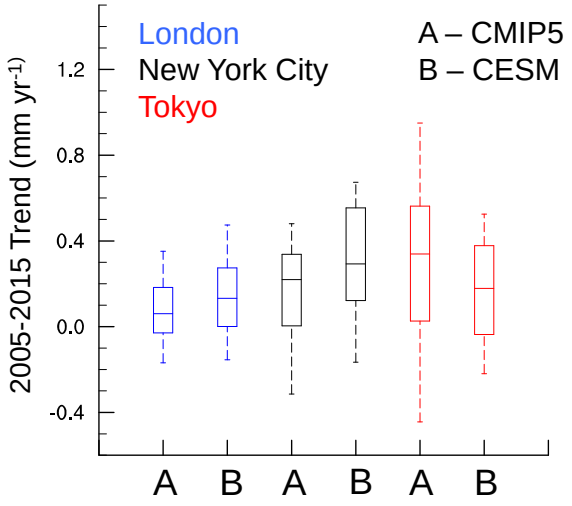

Figure 7. Box plots of steric sea-level trends over the full ocean column for three coastal locations. Notches from top to bottom represent 95% quantile, 75% quantile, median, 25% quantile, 5% quantile. Latitude and Longitudes used to calculate each set are as follows: London: 45–49° N, 346–6° E; Tokyo: 30–40° N, 134–145° E; New York City: 33–46° N, 280–290° E.

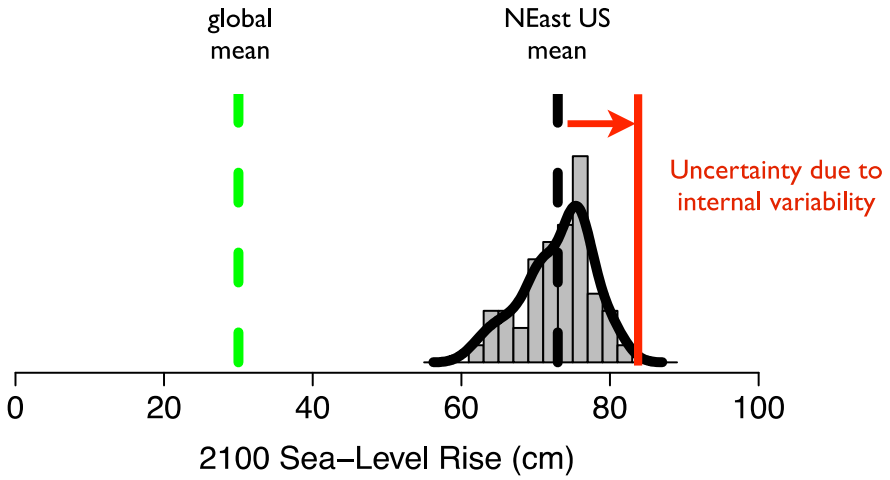

Figure 8. CESM ensemble spread of the total steric sea-level rise from 1850–2100 over the northeastern United States. The global mean total rise by this year is plotted as a dashed green line, northeastern ensemble mean as a black dashed line, and the upper bound of sea-level rise due to internal variability by the solid red line.

4. Conclusions

This study uses two types of Earth System Model ensembles, to quantify steric sea-level rise uncertainties in climate model ensembles due to internal ocean variability and structural model differences. The first (CESM) isolates the effect of internal variability of the coupled system (including the full ocean), and the second (CMIP5) samples the combined effect of structural model differences and internal variability. While CMIP5 displays larger ranges of steric sea-level rise than CESM at all depths and over all time periods considered, the internal variability exhibited by the CESM model contributes significantly to uncertainties in the total trends for both decadal and interdecadal time scales. On a global scale, variability in CMIP5 dominates, while on regional scales at important coastal locations, the magnitude of uncertainty due to internal variability in CESM is of a similar magnitude to the multi-model ensemble. These results have important implications for adaptation planning and coastal

resource management, as region-specific sea-level change provides more decision-relative information than global mean values. Here we show that uncertainties surrounding both internal variability and structural model differences can influence regional upper bound projections of sea-level rise.

Acknowledgments: This study was partially supported by the Department of Energy sponsored Program on Integrated Assessment Model Development, Diagnostics and Inter-Model Comparisons (PIAMDDI), and the Program on Coupled Human Earth Systems (PCHES). Any opinions, findings and conclusions or recommendations expressed in this material are those of the authors and do not necessarily reflect the views of the funding entities. We acknowledge the World Climate Research Programme's Working Group on Coupled Modelling, which is responsible for CMIP, and we thank the climate modeling groups (listed in Appendix A of this paper) for producing and making available their model output. For CMIP, the U.S. Department of Energy's Program for Climate Model Diagnosis and Intercomparison provides coordinating support and led development of software infrastructure in partnership with the Global Organization for Earth System Science Portals. We also acknowledge all sources of observations used in this study: observed sea-level rise from the National Centers for Environmental Information [40,41], observed atmospheric temperature from HadCRUT4 [48], and the sea-level change calculated by Llovel et al. (2014) [3], used as a guide for modeled changes calculated over the "Llovel Period".

Author Contributions: Both authors jointly designed the study and wrote the paper. Ryan Sriver performed the CESM simulations. Emily Hogan performed the model and data analyses.

Conflicts of Interest: The authors declare no conflict of interest. The founding sponsors had no role in the design of the study; in the collection, analyses, or interpretation of data; in the writing of the manuscript, and in the decision to publish the results.

Appendix A

We took the model run r1i1p1 from each of the CMIP5 model runs, and used the historical (1850–2005) and RCP 8.5 (2005–2100) simulations. Models in bold have fully interactive aerosol chemistry.

List of used CMIP5 models: ACCESS1-0, ACCESS1-3, bcc-csm1-1, bcc-csm1-1-m, BNU-ESM, CanESM2, CCSM4, CESM1-BGC, CESM1-CAM5, CMCC-CESM, CMCC-CM, CMCC-CMS, CNRM-CM5, CSIRO-Mk3-6-0, EC-EARTH, FGOALS-g2, FIO-ESM, GFDL-CM3, GFDL-ESM2G, GFDL-ESM2M, GISS-E2-H-CC, GISS-E2-R-CC, HadGEM2-CC, HadGEM2-ES, IPSL-CM5A-LR, IPSL-CM5A-MR, IPSL-CM5B-LR, MPI-ESM-LR, MPI-ESM-MR, NorESM1-M, NorESM1-ME.

More information on these models can be found on the CMIP5 website: http://cmip-pcmdi.llnl.gov/cmip5/index.html.

References

1. Church, J.A.; Clark, P.U.; Cazenave, A.; Gregory, J.M.; Jevrejeva, S.; Levermann, A.; Merrifield, M.A.; Milne, G.A.; Nerem, R.S.; Nunn, P.D.; et al. Sea Level Change. In *Climate Change 2013: The Physical Science Basis. Contribution of Working Group I to the Fifth Assessment Report of the Intergovernmental Panel on Climate Change*; Stocker, T.F., Qin, D., Plattner, G.-K., Tignor, M., Allen, S.K., Boschung, J., Nauels, A., Xia, Y., Bex, V., Midgley, P.M., Eds.; Cambridge University Press: Cambridge, UK; New York, NY, USA, 2013.
2. Rhein, M.; Rintoul, S.R.; Aoki, S.; Campos, E.; Chambers, D.; Feely, R.A.; Gulev, S.; Johnson, G.C.; Josey, S.A.; Kostianoy, A.; et al. Observations: Ocean (Chapter 3). In *Climate Change 2013: The Physical Science Basis. Contribution of Working Group I to the Fifth Assessment report of the Intergovernmental Panel on Climate Change*; Stocker, T.F., Qin, D., Plattner, G.-K., Tignor, M., Allen, S.K., Boschung, J., Nauels, A., Xia, Y., Bex, V., Midgley, P.M., Eds.; Cambridge University Press: Cambridge, UK; New York, NY, USA, 2013; pp. 255–315. [CrossRef]
3. Llovel, W.; Willis, J.K.; Landerer, F.W.; Fukumori, I. Deep-ocean contribution to sea level and energy budget not detectable over the past decade. *Nat. Clim. Chang.* **2014**, *4*, 1031–1035. [CrossRef]
4. Purkey, S.G.; Johnson, G.C. Warming of global abyssal and deep Southern Ocean waters between the 1990s and 2000s: Contributions to global heat and sea level rise budgets. *J. Clim.* **2010**, *23*, 6336–6351. [CrossRef]
5. Koutetsu, S.; Doi, T.; Kawano, T.; Masuna, S.; Sugiura, N.; Sasaki, Y.; Toyoda, T.; Igarashi, H.; Kawai, Y.; Katsumata, K.; et al. Deep ocean heat content changeds estimated from observation and reanalysis product and their influence on sea level change. *J. Geophys. Res.* **2011**, *116*, 869–881.
6. Gille, S.T. Warming of the Southern Ocean since the 1950s. *Science* **2002**, *295*, 1275–1277. [CrossRef] [PubMed]

7. Gille, S.T. Decadal-scale temperature trends in the Southern Hemisphere ocean. *J. Clim.* **2008**, *21*, 4749–4765. [CrossRef]
8. AchutaRao, K.M.; Ishii, M.; Santer, B.D.; Gleckler, P.J.; Taylor, K.E.; Barnett, T.P.; Pierce, D.W.; Stouffer, R.J.; Wigley, T.M.L. Simulated and observed variabilty in ocean temperature and heat content. *Proc. Natl. Acad. Sci. USA* **2007**, *104*, 10768–10773. [CrossRef] [PubMed]
9. Gouretski, V.; Koltermann, K.P. How much is the ocean really warming? *Geophys. Res. Lett.* **2007**, *34*, L01610. [CrossRef]
10. Domingues, C.M.; Church, J.A.; White, N.J.; Gleckler, P.J.; Wijffels, S.E.; Barker, P.M.; Dunn, J.R. Improved estimates of upper-ocean warming and multi-decadal sea-level rise. *Nature* **2008**, *453*, 1090–1093. [CrossRef] [PubMed]
11. Durack, P.J.; Gleckler, P.J.; Landerer, F.W.; Taylor, K.E. Quantifying Underestimates of Long-term Upper-Ocean Warming. *Nat. Clim. Chang.* **2014**, *4*, 999–1005. [CrossRef]
12. Cheng, L.; Zhu, J.; Abraham, J. Global Upper Ocean Heat Content Estimation: Recent Progress and the Remaining Challenges. *Atmos. Ocean. Sci. Lett.* **2015**, *8*, 333–338. [CrossRef]
13. Cheng, L.; Zhu, J.; Trenberth, K.E.; Fasullo, J.; Boyer, T.; Abraham, J. Improved estimates of ocean heat content from 1960 to 2015. *Sci. Adv.* **2017**, *3*, e1601545. [CrossRef] [PubMed]
14. Sriver, R.L.; Urban, N.M.; Olson, R.; Keller, K. Towards a physically plausible upper bound of sea-level rise projections. *Clim. Chang.* **2012**, *115*, 893–902. [CrossRef]
15. Buchanan, M.K.; Kopp, R.E.; Oppenheimer, M.; Tebaldi, C. Allowances for evolving coastal flood risk under certain local sea-level rise. *Clim. Chang.* **2016**, *137*. [CrossRef]
16. Kopp, R.E.; Horton, B.P.; Kemp, A.C.; Tebaldi, C. Past and future sea-level rise along the coast of North Carolina. *Clim. Chang.* **2015**, *132*, 637–707. [CrossRef]
17. Cazenave, A.; Le Cozannet, G. Sea level rise and its coastal impacts. *Earths Future* **2014**, *2*, 15–34. [CrossRef]
18. Liang, X.; Wunsch, C.; Heimback, P.; Forget, G. Vertical redistrubution of oceanic heat content. *J. Clim.* **2015**, *28*, 3821–3833. [CrossRef]
19. Kuhlbrodt, T.; Gregory, J.M. Ocean heat uptake and its consequences for the magnitude of sea level rise and climate change. *Geophys. Res. Lett.* **2012**, *39*, L18608. [CrossRef]
20. Hu, A.; Deser, C. Uncertainty in future regional sea level rise due to internal climate variability. *Geophys. Res. Lett.* **2013**, *40*, 2768–2772. [CrossRef]
21. Flato, G.; Marotzke, J.; Abiodun, B.; Braconnot, P.; Chou, S.C.; Collins, W.; Coz, P.; Driouech, F.; Emori, S.; Eyring, C.; et al. Evaluation of Climate Models. In *Climate Change 2013: The Physical Science Basis. Contribution of Working Group I to the Fifth Assessment Report of the Intergovernmental Panel on Climate Change*; Stocker, T.F., Qin, D., Plattner, G.K., Tignor, M., Allen, S.K., Boschung, J., Nauels, A., Xia, Y., Bex, V., Midgley, P.M., Eds.; Cambridge University Press: Cambridge, UK; New York, NY, USA, 2013.
22. Thompson, D.W.K.; Barnes, E.A.; Deser, C.; Foust, W.E.; Phillips, A.S. Quantifying the role of internal calimte variability in future climate trends. *J. Clim.* **2015**, *28*, 6443–6456. [CrossRef]
23. Sriver, R.L.; Forest, C.E.; Keller, K. Effects of intial conditions uncertainty on regional climate variability: An analysis using a low resolution CESM ensemble. *Geophys. Res. Lett.* **2015**, *42*, 5468–5476. [CrossRef]
24. Taylor, K.E.; Stouffer, R.J.; Meehl, G.A. An overview of CMIP5 and the experiment design. *Bull. Am. Meteorol. Soc.* **2012**, *93*, 485–495. [CrossRef]
25. Deser, C.; Phillips, A.; Bourdette, V.; Tend, H. Uncertainty in climate change projections: the role of internal variability. *Clim. Dyn.* **2012**, *38*, 527–547. [CrossRef]
26. Kay, J.; Deser, C.; Phillips, A.; Mai, A.; Hannay, C.; Strand, G.; Arblaster, J.M.; Bates, S.C.; Danabasoglu, G.; Edwards, J.; et al. The Community Earth System Model (CESM) Large Ensemble Project: A community resource for studying climate change in the presence of internal climate variability. *Bull. Am. Meteorol. Soc.* **2015**, *96*, 1333–1349. [CrossRef]
27. Fischer, E.M.; Beyrerle, U.; Knutti, R. Robust spatially aggregated projections of climate extremes. *Nat. Clim. Chang.* **2013**, *3*, 1033–1038. [CrossRef]
28. Fasullo, J.T.; Nerem, R.S. Interannual variability in global mean sea level estimated from the CESM Large and last millennium ensembles. *Water* **2016**, *8*, 491. [CrossRef]
29. Fyfe, J.C.; Gillett, N.P.; Zwiers, F.W. Overestimated global warming over the past 20 years. *Nat. Clim. Chang.* **2013**, *3*, 767–769. [CrossRef]

30. Huang, J.; Xie, Y.; Guan, X.; Li, D.; Ji, F. The dynamic of the warming hiatus over the Northern Hemisphere. *Clim. Dyn.* **2016**, *48*, 429–446. [CrossRef]
31. Easterling, D.R.; Wehner, M.F. Is the climate warming or cooling? *Geophys. Res. Lett.* **2009**, *36*, L08706. [CrossRef]
32. Meehl, G.A.; Arblaster, J.M.; Fasullo, J.T.; Hu, A.; Trenberth, K.E. Model-based evidence of deep-ocean heat uptake during surface-termpertaure hiatus periods. *Nat. Clim. Chang.* **2011**. [CrossRef]
33. Kosaka, Y.; Xie, S.P. Recent global-warming hiatus tied to equatorial Pacific surface cooling. *Nature* **2013**, *501*, 403–407. [CrossRef] [PubMed]
34. Trenberth, K.E.; Fasullo, J.T. An apparent hiatus in global warming? *Earths Future* **2013**, *1*, 19–32. [CrossRef]
35. Trenberth, K.E.; Fasulo, J.T.; Branstator, G.; Phillips, A.S. Seasonal aspects of the recent pause in surface warming. *Nat. Clim. Chang.* **2014**. [CrossRef]
36. Levitus, S.; Antonov, J.I.; Boyer, T.P.; Baranova, O.K.; Garcia, H.; Locarnini, R.A.; Mishonov, A.V.; Reagan, J.R.; Seidov, D.; Yarosh, E.S.; et al. World ocean heat content and thermosteric sea level change (0–2000 m), 1955–2010. *Geophys. Res. Lett.* **2012**, *39*, L10603. [CrossRef]
37. Griffies, S.M.; Winton, M.; Anderson, W.G.; Benson, R.; Delworth, T.L.; Dufour, C.O.; Dunne, J.P.; Goddard, P.; Morrison, A.K.; Rosati, A.; et al. Impacts on ocean heat from transient mesoscale eddies in a hierarchy of climate models. *J. Clim.* **2015**, *28*, 952–977. [CrossRef]
38. Hawkins, E.; Sutton, R. The potential to narrow uncertainty in regional climate predictions. *Bull. Am. Meteorol. Soc.* **2009**, *90*, 1095–1107. [CrossRef]
39. Hawkins, E.; Sutton, R. The potential to narrow uncertainty in projections of regional precipitation change. *Clim. Dyn.* **2011**, *37*, 407–418. [CrossRef]
40. Boyer, T.P.; Antonov, J.I.; Baranova, O.K.; Garcia, H.E.; Johnson, D.R.; Locarnini, R.A.; Mishonov, A.V.; O'Brien, T.D.; Seidov, D.; Smolyar, I.V.; et al. World Ocean Database 2009, Volume 1, Introduction. In *NOAA Atlas NESDIS*; Levitus, S., Ed.; NOAA: Silver Spring, MD, USA, 2009.
41. National Centers for Environmental Information, National Oceanic and Atmospheric Administration. Available online: https://www.ncei.noaa.gov/ (accessed on 28 June 2017).
42. Shields, C.A.; Bailey, D.A.; Danabasoglu, G.; Kiehl, J.T.; Levis, S.; Jochum, M.; Park, S. The low-resolution CCSM4. *J. Clim.* **2012**, *25*, 3993–4014. [CrossRef]
43. Gent, P.R.; Danabasoglu, G.; Donner, L.J.; Holland, M.M.; Hunke, E.C.; Jayne, S.R.; Lawrence, D.M.; Neale, R.B.; Rasch, P.J.; et al. The Community Climate System Model Version 4. *J. Clim.* **2011**, *24*, 4973–4991. [CrossRef]
44. Smith, R.D.; Jones, P.; Briegleb, B.; Bryan, F.; Danabasoglu, G.; Dennis, J.; Dukowicz, J.; Eden, C.; Fox-Kemper, B.; Gent, P.; et al. *The Parallel Ocean Program (POP) Reference Manual: Ocean Component of the Community Climate System Model (CCSM)*. LANL Technical Report, LAUR-10-01853. Available online: https://staff.ucar.edu/browse/people/11128/manuscripts%3A825 (accessed on 1 July 2017).
45. Moss, R.H.; Edmonds, J.A.; Hibbard, K.A.; Manning, M.R.; Rose, S.K.; van Vuuren, D.P.; Carter, T.R.; Emori, S.; Kainuma, M.; Kram, T.; et al. The next generation of scenarios for climate change research and assessment. *Nature* **2010**, *463*, 747–756. [CrossRef] [PubMed]
46. Bitz, C.M.; Shell, K.M.; Gent, P.R.; Bailey, D.; Danabasoglu, G.; Armour, K.C.; Holland, M.M.; Kiehl, J.T. Climate Sensitivity of the Community Climate System Model Version 4. *J. Clim.* **2012**. [CrossRef]
47. Chylek, P.; Vogelsang, T.J.; Klett, J.D.; Hengartner, N.; Higdon, D.; Lesins, G.; Dubey, M.K. Indirect aerosol effect increases CMIP5 models' projected arctic warming. *J. Clim.* **2016**. [CrossRef]
48. Morice, C.P.; Kennedy, J.J.; Rayner, N.A.; Jones, P.D. Quantifying uncertainties in global and regional temperature change using an ensemble of observational estimates: The HadCRUT4 dataset. *J. Geophys. Res.* **2012**, *117*, D08101. [CrossRef]
49. Yin, J.J.; Schlesinger, M.E.; Stouffer, R.J. Model projections of rapid sea-level rise on the northeast coast of the United States. *Nat. Geosci.* **2009**, *2*, 262–266. [CrossRef]
50. McDougall, T.J.; Jackett, D.R.; Wright, D.G.; Feistel, R. Accurate and computationally efficient algorithms for potential temperature and density of sea water. *J. Atmos. Ocean. Tech.* **2003**, *20*, 730–741. [CrossRef]
51. Gupta, A.S.; Muir, L.C.; Brown, J.N.; Phipps, S.J.; Durack, P.J.; Monselesan, D.; Wijffels, S.E. Climate drift in the CMIP3 models. *J. Clim.* **2012**, *25*, 4621–4640. [CrossRef]
52. Lorbarcher, K.; Nauels, A.; Meinshausen, M. Complementing thermosteric sea level rise estimates. *Geosci. Model. Dev.* **2015**, *8*, 2723–2734. [CrossRef]

53. Bilbao, R.A.F.; Gregory, J.M.; Bouttes, N. Analysis of the regional pattern of sea level change due to ocean dynamics and density change for 1993–2099 in observations and CMIP5 AOGCMs. *Clim. Dyn.* **2015**, *45*, 2647–2666. [CrossRef]
54. Roemmich, D.; Owens, W.B. The Argo Project: Global ocean observations for understanding and prediction of climate variability. *Oceanography* **2000**, *13*, 45–50. [CrossRef]
55. Tapley, B.D.; Bettadpur, S.; Rise, J.C.; Thompson, P.F.; Watkins, M. GRACE measurements of mass variability in the Earth system. *Science* **2004**, *305*, 503–505. [CrossRef] [PubMed]
56. Leuilette, E.W.; Nerem, R.S.; Mitchum, G.T. Calibration of TOPEX/Posidon and Jason altimeter data to construct a continuous record of mean sea level change. *Mar. Geod.* **2004**, *27*, 79–94. [CrossRef]
57. Dieng, H.B.; Cazenave, A.; von Schuckmann, K.; Albain, M.; Meyssignac, B. Sea level budget over 2005–2013: Missing controbutions and data errors. *Ocean Sci.* **2015**, *12*, 701–734. [CrossRef]
58. Von Schuckmann, K.; Sallée, J.B.; Chambers, D.; Le Traon, P.-Y.; Cabanes, C.; Gaillard, F.; Speich, S.; Hamon, M. Consitency of the current global ocean observing systems from an Argo perspective. *Ocean Sci.* **2014**, *10*, 547–557. [CrossRef]
59. Lempert, R.; Sriver, R.L.; Keller, K. Characterizing uncertain sea level rise projections support infrastructure investment decisions. *Calif. Energy Comm.* **2012**. Available online: http://www.energy.ca.gov/2012publications/CEC-500-2012-056/CEC-500-2012-056.pdf (accessed on 1 July 2017).